Combining Chemical and Dynamical Measurements to Delineate the Interplay between Dynamical Forcings and Global Pollution

Weizhi Deng[1], Jason Blake Cohen[1], Shuo Wang[1], and Chuyong Lin[1]

[1]School of Atmospheric Sciences, Sun Yat-Sen University

November 26, 2022

Abstract

This work addresses the relationship between major dynamical forcings and variability in NO column measurements. The dominating impact on Siberia is due to El Niño, on Indonesia, Northern Australia and South America is due to IOD,and on the remaining regions is due to NAO. That NO pollution in Indonesia is modulated by IOD contradicts previous work using AOD and El Niño. Simultaneous impacts of present and lagged forcings are derived using multi-linear regression, demonstrating El Niño impacts NO variability from 7 to 98 weeks ahead, while IOD and NAO are mostly impacted by past changes in NO variability. In all cases, lagged forcings exhibit more impact than present forcings, hinting at non-linearity. Finally, dynamical forcings are responsible for over 50% of the NO variability in most non-urban areas and over 40% in urban Indonesia and China. These results demonstrate the significance of climate forcing on short-lived air pollutants.

Combining Chemical and Dynamical Measurements to Delineate the Interplay between Dynamical Forcings and Global Pollution

Weizhi Deng[1], Jason Blake Cohen[1,2,*], Shuo Wang[1], Chuyong Lin[1]

[1]School of Atmospheric Sciences, Sun Yat-Sen University.

[2]Southern Marine Science and Engineering Guangdong Laboratory (Zhuhai).

[*]Corresponding author: Jason Blake Cohen (jasonbc@alum.mit.edu)

Key Points:

- El Niño impacts NO_2 pollution in Siberia; IOD in Indonesia, Northern Australia, and South America; and NAO in the rest of the world.
- Dynamical forcings are responsible for over 50% of the NO_2 variability in non-urban areas and over 40% in urban Indonesia and China.
- Lagged dynamical forcings dominate present forcings on NO_2 pollution, with El Niño 7 to 98 weeks forward, while IOD and NAO are past.

Abstract: This work addresses the relationship between major dynamical forcings and variability in NO_2 column measurements. The dominating impact on Siberia is due to El Niño, on Indonesia, Northern Australia and South America is due to IOD, and on the remaining regions is due to NAO. That NO_2 pollution in Indonesia is modulated by IOD contradicts previous work using AOD and El Niño. Simultaneous impacts of present and lagged forcings are derived using multi-linear regression, demonstrating El Niño impacts NO_2 variability from 7 to 98 weeks ahead, while IOD and NAO are mostly impacted by past changes in NO_2 variability. In all cases, lagged forcings exhibit more impact than present forcings, hinting at non-linearity. Finally, dynamical forcings are responsible for over 50% of the NO_2 variability in most non-urban areas and over 40% in urban Indonesia and China. These results demonstrate the significance of climate forcing on short-lived air pollutants.

Plain Language Summary

We examine the relationships between three important sources of climate variability over the past decade: El Niño, IOD, and NAO, and rapid changes in the atmospheric amounts of the short-lived air pollutant NO_2. The climate forcings give us examples of how the changes in the climate state may impact air pollution in the future, while the air pollution is selected as a proxy for urbanization and wildfires. The major regions of change of air pollution are related to the changes in the climate variability, with different forcings impacting different regions, and all regions are significantly impacted by at least one forcing. We further determine that past changes in El Niño impact the present-day pollution, and that the present-day pollution also impacts future changes in IOD and NAO. Finally, we determine that climate impacts over 40% of the change in air pollution in urban areas of Asia, and over 50% of the change in air pollution elsewhere. Therefore, we urge more attention to the impacts that future climate change is expected to have on air pollution.

Key words:

El Niño, Indian Ocean Dipole (IOD), North Atlantic Oscillation (NAO), NO_2 column measurements, variability

1. Introduction

Present approaches address the issue of a one-way impact of either the changes in large-scale average air pollution on the meteorology, or changes in the large-scale meteorology on the air pollution loadings (Chen et al., 2019b; Knippertz et al., 2015; Shen et al., 2017). Some studies have looked into the contribution from non-linear aspects in terms of large-scale overall changes that one system may have on the other system (Bollasina et al., 2011). To accomplish these goals, papers have used idealized perturbations of emissions with known past reanalysis or highly-constrained future meteorology and/or climatology (Cohen & Wang, 2014; Dewitt et al, 2019). Other studies have looked at the impact of well-known dynamical perturbations on fixed emissions, using both past and future meteorology, based on different future climate perturbations (Bollasina et al., 2013; Kim et al., 2017; Persad et al., 2014). There have been a small number of studies that have tried to look at the interactive changes, on a season-to-season scale, that occur between known urban pollution events and the climatology (Cohen, 2014; Cohen et al., 2011; Grandey et al., 2019; Guo et al., 2019).

However, this past research has not been capable of allowing us to understand the largest and most polluted events, such as annually occurring extreme biomass burning events in Africa, South America, and Southeast Asia each year that are known to lead to pollution levels many times larger than the average pollution levels known to occur in heavily polluted cities (Aragão et al., 2018; Cohen, 2014; Cohen & Wang, 2014; Cohen et al., 2018; Ichoku et al., 2008; Lin et al., 2019). As a community we still cannot explain such differences as why there are vast differences between the clean and polluted seasons in some regions that have a high annual pollution loading such as China, India, and Southern Africa (Chen et al., 2019b; Jin & Wang, 2017). Furthermore, we have no way to do any sort of prediction in terms of why regions which are normally relatively clean, such as Singapore and London, can occasionally record PM2.5 levels higher than any other city on the planet (Velasco & Rastan, 2015; Wilkins, 1954). In addition to missing these extreme events, when extreme events are predicted by models tend to also not concur with the real timing of when such events occur, with the current generation of models and forecasts clearly having a mis-representation in terms of the timing of extreme events (Cohen & Wang, 2014; Lan et al., 2019).

One of the major underlying issues at hand is that we are not clear as to what the major or most important factors are contributing to extreme air pollution events (Chen et al., 2019a). It is well known that models are not capable of capturing the actual El Niño signal (DiNezio et al., 2017). El Niño is a coupled atmospheric and oceanic phenomenon that influences the distribution of heat, energy, and moisture throughout the tropical atmosphere. Its impact is found to occur over the tropics around the entire world, as well as in mid-latitude zones in southern South America and Eastern US (Diaz & Markgraf, 2000). This phenomenon also has a strong inter-annual variation, with the largest influence over the past three decades occurring in 1997 and 2015.

While there has been a significant amount of work focusing on El Niño and its impact on wildfires in Indonesia (Cohen, 2014; Field et al., 2016; Reid el al., 2012; Siegert et al., 2001; Sun et al., 2013; Tosca et al., 2011), there are currently no modeling studies that have been able to dynamically link these two extremes together (Leung et al., 2007; Martin et al., 2012; Tsigaridis et al., 2014).

Two other important dynamical phenomena also addressed include the Indian Ocean Dipole (IOD) and the North Atlantic Oscillation (NAO). The former is known to be a significant source of climate variability in Indian Ocean that modulates the atmospheric circulation all over the globe (Saji et al., 1999). The latter impacts areas stretching from the Eastern United States to Siberia, and from the Arctic to the Subtropical Atlantic (Hurrell, 1995; Hurrell et al., 2003).

For these reasons, we will strive to integrate measurements of drivers of extreme events from both the chemical and dynamical forcing perspectives, and investigate how these are coupled to each other. By using real remotely sensed and reanalysis data products, at high frequency, we can capture the relationship between the air pollution and dynamical extremes. Our focus is on those regions which are rapidly changing, or have large-scale variability inter-annually or intra-annually. The reason for this is to aim for our ability to make recommendations in terms of how to achieve co-benefits or account for co-costs of the changing air pollution and climate systems, with a focus on large-scale biomass burning and the growth of new urban regions.

2.Data and Methods

2.1 Geography

This study explores the impacts that some significant dynamical drivers of the climate system have on various regions of highly variable air pollution found throughout the world over the past 15 years. In order to better understand how meteorology and air pollution interplay over different parts of the globe, we group the world according to the role the meteorological drivers play, as well as the timing and loading patterns of the air pollution measurements. This process looks globally at the data, while ensuring that each region is both spatially and temporally orthogonal. In addition, geographical considerations are taken into account to group things which have underlying similarities. Results of various dynamical and air pollution classifications will be elaborated upon at a later point.

2.2 Air Pollution Data

To represent air pollution, we employ a weekly average dataset of remotely sensed, cloud filtered NO_2 columns. This product is derived from daily NO_2 tropospheric column measurements, with a spatial resolution of 13km by 24km, from the version 3 Level 2 cloud screened Ozone Monitoring Instrument (OMI) satellite product. We further adapt a variance maximization filter to represent those regions undergoing the most change over the time period from January 2006 through December 2015, as shown in **Figure 1a** and **Table S1**. This combination guarantees that we have found those regions which are undergoing either intense annual or interannually varying fires, or other long-term urban changes (Lan et al., 2019; Lin et al., 2019). As observed in the time series of the absolute magnitude of NO_2 column loading over these 13 maximal regions in this work (**Figures 1b1-1b5**) the peak values range from 1.7 to 6.0 times higher than the median, with a duration from 1 to 11 weeks a year (based on a normalized cutoff of 1.5). These peaks occur annually (except for Siberia and Western US and Canada) and contain a considerable amount of inter- and intra-annual variation.

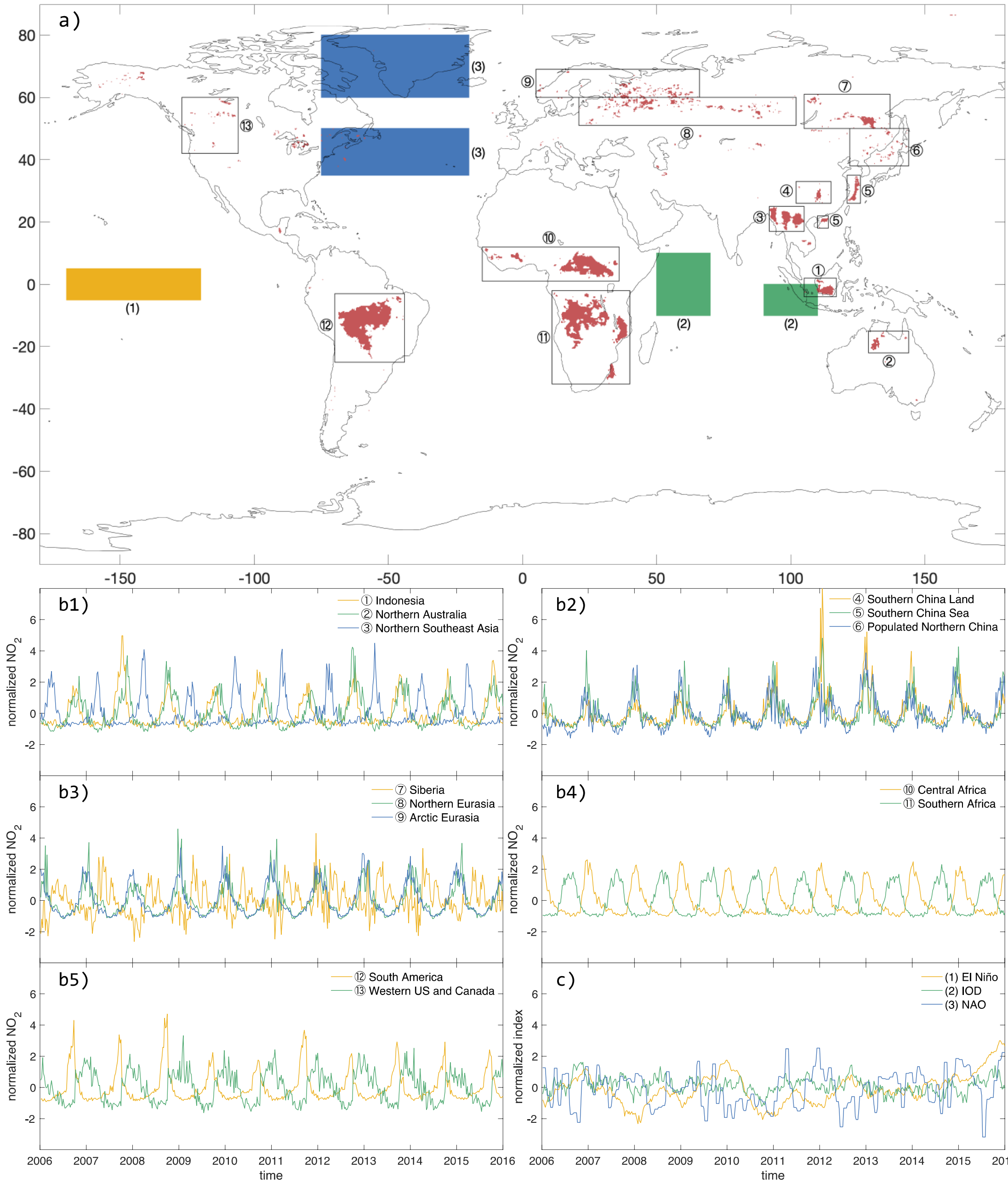

Figure 1: **(a)** Global distribution of the most significant regions of NO_2 variation (black outlines with red colors) and dynamical forcings (single-colored boxes: El Niño yellow, IOD green, and NAO blue) as in **Table S1**. Time series of normalized weekly OMI

NO_2 over: **(b1)** Southeast Asia and Australia, **(b2)** East Asia, **(b3)** Eurasia, **(b4)** Africa, and **(b5)** the Americas. **(c)** Time series of normalized weekly NOAA climate indices.

2.3 Climate Data

The specific dataset we employ here to represent El Niño is the weekly data from the NOAA Ocean Observation Panel for Climate (OOPC) dataset, as shown in **Figure 1a,c.** We specifically use the region referred to Niño3.4, which is based on the measurements of Sea Surface Temperature (SST) over the tropical regions bounded by 170°W to 120°W, and 5°S to 5°N. Furthermore, the strong interannual variation is observed to have two significant peaks (in 2009 and 2015) and one weak peak (in 2006) over the period studied here.

The specific dataset used to represent the IOD is the Dipole Mode Index (DMI) obtained from the NOAA OOPC, also shown in **Figure 1a,c**. The DMI is calculated by the SST anomaly difference between the western and southeastern tropical Indian Ocean regions (50°E - 70°E and 10°S - 10°N) and (90°E - 110°E and 10°S - 0°) respectively (Saji et al., 1999). The climate variability casts its greatest impact on tropical Indian Ocean, peaking in the years 2006, 2008, 2012, 2015 and reaching its nadir in 2010 over the past 15 years.

The specific dataset used for the NAO is the monthly NOAA Climate Prediction Center NAO index. This is calculated as the leading component of rotated empirical orthogonal function of 500mb geopotential height north of 20°N, centered over the Atlantic Ocean. The NAO has its largest impact over Greenland and the Subtropical Atlantic Ocean, and exhibits great intra-annual variability, with the largest peak and trough over this study being in 2011 and 2015 respectively.

We linearly interpolate the NAO index to a weekly frequency to be consistent with the other datasets used in the work, and include the values from 2006 to 2015, as shown in **Figure 1a,c**. The spatial distribution employed is based on the July loading map, spanning the three most positive and negative regions at (NOAA Climate Prediction Center Internet Team, 2005). We specifically choose the July map since it represents a decent compromise between the maximum spatial response in January and the minimum spatial response in October.

2.4 Analytics

2.4.1 Variance Maximization

To consider only those regions which are undergoing the most significant amount of NO_2 change, we employ a normalized standard deviation maximization approach. This approach is further refined by filtering the data to ensure that the difference between the localized mean and the mean of the peak conditions are separated by a factor of at least 2 standard deviations. Finally, the data is filtered so that it has a local maximum value which is at least as great as 2 times the global annual mean value. More details can be found in Cohen, 2014 and Lan et al., 2019.

2.4.2 Correlation and Regression

We employ a t-test for means of a linear correlation between different datasets. In all cases we require that the p value be smaller than 0.05 to be considered successful. We exclude all cases where the absolute value of the R statistic is smaller than 0.10.

In the case of least squares multiple linear regression to fit multiple air pollution and dynamical datasets simultaneously, we require that the p value be smaller than 0.05 to be successful. We also only include those terms which contribute at least 10 percent to the normalized final best fit result.

3. Results

3.1 Correlations between NO_2 and Dynamical Forcings

We compute the correlation coefficient between the weekly NO_2 column measurements and each of the weekly indices of the three dynamical forcings respectively spanning the period of study. Global maps of this impact over regions which have an R value with an absolute value greater than 0.1 are given in **Figure 2**.

We find that El Niño has an impact over the tropical belt stretching from Northern Southeast Asia to Africa. Extra-tropical areas impacted include Eastern China, Japan, Northern Australia and Eastern United States. However, we do not find a statistically significant impact of El Niño on the NO_2 column loadings in Indonesia, which is contradictory to many other previous published works showing El Niño as the major driving force of fires occurring in the Maritime Continent (Marlier et al., 2013; Reid et al., 2012).

The impact of the IOD occurs throughout tropical areas stretching from Indonesia, to Africa and further onto South America. In addition to this, subtropical areas including Eastern China and Japan are also impacted. It is worth mentioning that there is a belt over the Indian Ocean as observed in **Figures 2a,b** in which both El Niño and the IOD have an aligned congruence in phase. This is possibly associated with long-range transport of smoke from fires, as has been observed in other parts of Asia (Lin et al. 2019; Sun et al., 2013), although there is no known work demonstrating this over the Southern Indian Ocean.

The impact of the NAO is felt over most parts of the world in a wavelike manner. It is interesting to note that the impacts from the NAO seem to not be spatially correlated with either of those from the previous two forcings in general, although there are significant areas of overlap between both regions at the same phase as well as the opposite phase, leading to addition and subtraction respectively.

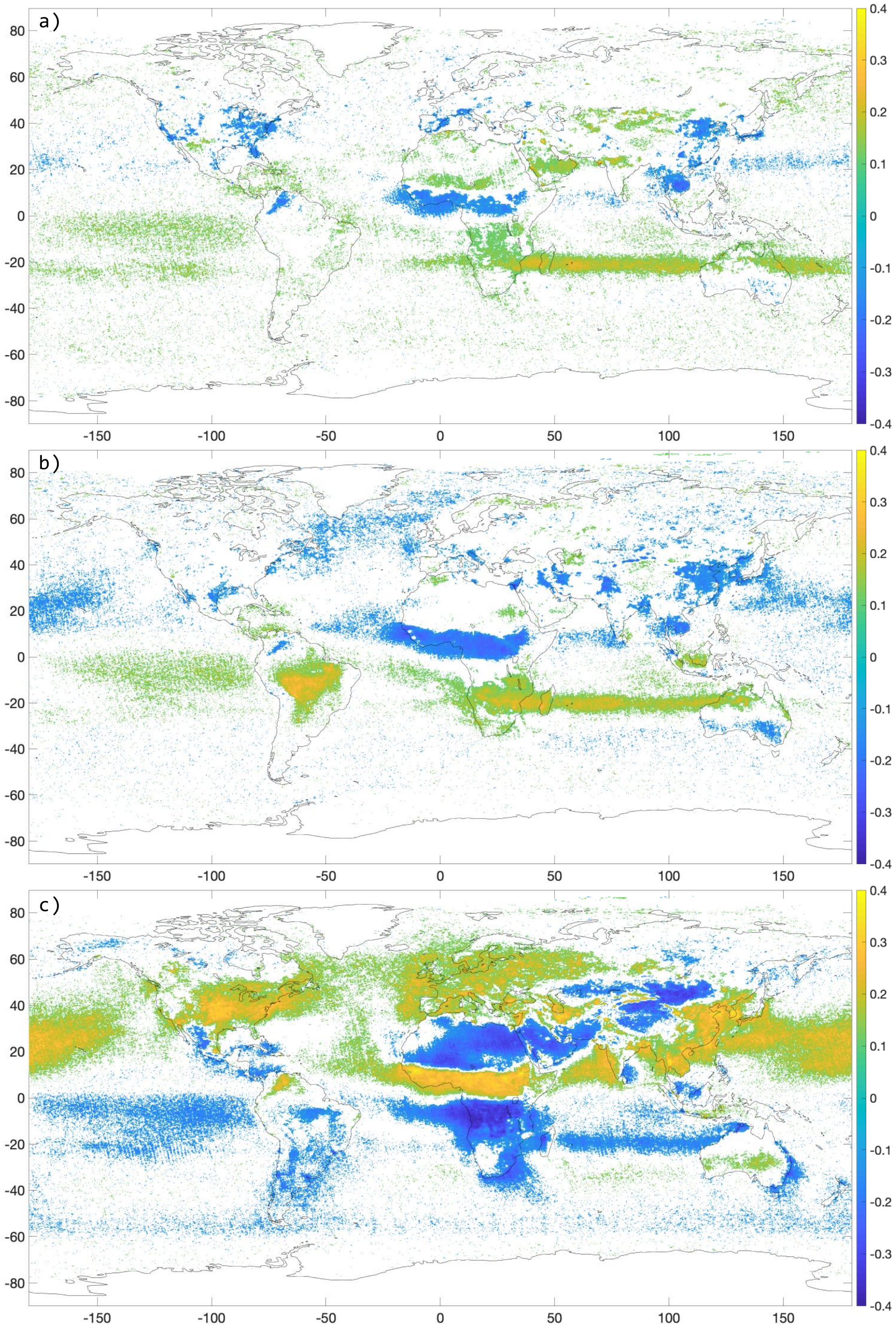

Figure 2: Map of regions with a statistically significant correlation coefficient between weekly column NO_2 measurements and the respective indices for: **(a)** El Niño, **(b)** IOD, and **(c)** NAO.

To examine which dynamical forcings are modulating or interacting with the regions of highest variations in NO_2 loadings, we choose to look at each of the 13 classified regions individually (as given in **Figure 1** and **Table S1**). First, we observe that the El Niño is the sole dynamical pattern having an impact in Siberia. It is also found to make a difference over Northern Australia, Northern Southeast Asia, Southern China Land and Sea, Northern Eurasia and Western United States and Canada, with the absolute value of R greater than 0.10.

Second, the IOD plays a dominant role in Indonesia, Northern Australia and South America. Specifically, we notice that the IOD is dominating the correlation over Indonesia, with R as high as 0.21. This stands in stark contrast to some previous findings that El Niño dominates the dynamical forcing in this region (Marlier et al., 2013; Reid et al., 2012). In fact, the correlation coefficient between El Niño and averaged NO_2 over Indonesia does not even pass the t-test. This contradiction may be due to a few things. Firstly, previous studies used monthly dynamical and AOD data, whereas we are employing weekly data. Secondly, we are using NO_2, which has a shorter life time than aerosols in-situ and therefore does not flow as far from the source region as aerosols. Our approach focuses on the source region only, not the combined source and downwind regions of transport.

Third, we observe that the NAO has a significant impact over most of the regions, including Northern Southeast Asia, Southern China Sea and Land, Populated Northern China, Northern and Arctic Eurasia, Central and Southern Africa and Western United States and Canada. Over these regions, the absolute value of R is always larger than 0.20. It is worth mentioning that over Populated Northern China, the NAO is dominant (with R as high as 0.25), consistent with previous work (Chen et al., 2019b).

All three dynamical forcings seem to converge over Central and Southern Africa, with there being a significant correlation between each individual forcing and the NO_2 over the regions. Overall, the NAO seems is slightly more dominant, with the IOD having the second strongest contribution, and El Niño the weakest. However, the timing and loading patterns of the NO_2 over these two regions respond in the opposite direction to each other, and hence all three climate variables. This anti-correlation signal is due to the fact that the two regions are located in different hemispheres and thus also influenced by the movement of the Intertropical Convergence Zone (ITCZ).

3.2 Developing a Multi-Linear Model of NO_2 Concentrations from Different Present-day and Lagged Dynamical Forcings

We first use the extended dynamical time series from 2004 to 2017 to quantify the idealized lag time between each dynamical forcing and NO_2 measurement, assuming a maximum of a two-year lag. The time lag is chosen so as to maximize the correlation between the dynamical forcing and the NO_2 measurements. The results are given in **Table 1**.

On one hand, we observe that El Niño exclusively impacts future loadings of NO_2 over all studied regions. This is because when the dry-phase extreme occurs, it makes the associated region more prone to enhanced fire in the future, and visa verse for the wet-phase extreme. On the other hand, the IOD and NAO are found to lag behind the NO_2 measurements over almost all studied areas, which means that NO_2 or other co-emitted species produced by the fires (such as aerosols) may pose a significant feedback onto the energy balance or dynamics underlying these forcings.

Next we employ a statistical multi-linear regression approach over each individual region, to quantify the measured NO_2 as a weighted function of the Niño3.4, DMI, and NAO indices, both with and without a time lag respectively. The resulting coefficients and R square values of the multi-linear regression are also listed in **Table 1**. The point is to quantify which dynamical systems play the largest role in modulating NO_2 from these rapidly varying regions, when considering both their magnitude and their maximum lag, in combination with each other as felt in the true environment where these forcings are not clearly separated from each other.

First, we find that the lagged dynamical forcings are at least as important as the present-day dynamical forcings in all cases. Specifically, lagged El Niño and lagged NAO make a significant difference in all regions studied, while the lagged IOD makes a difference in all regions, except for Northern Southeast Asia and South America. Second, we find present-time dynamical forcings generally exhibit a weaker coefficient. For instance, the unlagged El Niño makes an impact only on Northern Southeast Asia, the unlagged IOD makes an impact solely on Indonesia, Northern and Arctic Eurasia, and Central and Southern Africa, while the unlagged NAO makes an impact on Northern Southeast Asia, Southern China Sea, Populated Northern China, Northern and Arctic Eurasia, Central and Southern Africa and the Western United States and Canada. Additionally, apart from impacting more regions, the lagged terms also yield their highest magnitude everywhere other than the IOD term in South America.

Furthermore, the multi-linear regression model fit is superior to the individual correlations over all regions, with the greatest improvement in R^2 ranging from 0.09 to 0.37. In fact, the multi-linear regression model fit is very capable of reproducing the normalized standard deviation of the measured OMI NO_2 column loadings over the regions of interest presented here, as observed in **Figure 3**. In specific, this approach is able to reproduce at least half of the known variability in regions which have been previously shown to be highly impacted by one or more of these dynamical systems (Aragão et al., 2018; Ichoku et al., 2008; Lan et al., 2019; Lin et al., 2019; Sun et al., 2013). Three of the four regions not meeting this threshold have a large fraction (over 40 percent) of their total variability due to high levels of urbanization (Indonesia and China).

	Region	El Niño	IOD	NAO	b0	b1	b2	b3	b4	b5	b6	R^2
1	Indonesia	87	-16	-40	-0.06	-0.07	0.21	-0.05	-0.22	-0.26	-0.29	0.29
2	Northern Australia	91	5	-87	-0.13	0.03	0.04	0.07	-0.37	0.26	-0.34	0.31
3	Northern Southeast Asia	7	-25	-67	-0.04	0.38	-0.07	0.13	-0.50	0.09	-0.33	0.26
4	Southern China Land	48	-6	-52	-0.04	-0.07	-0.08	0.10	-0.37	-0.21	0.34	0.28
5	Southern China Sea	47	-5	-30	-0.05	-0.05	-0.07	0.20	-0.29	-0.14	-0.32	0.31
6	Populated Northern China	25	-7	22	0.04	0.01	0.05	0.15	0.13	-0.20	-0.25	0.20
7	Siberia	65	-32	-57	-0.03	0.06	-0.03	-0.04	-0.20	-0.14	-0.19	0.13
8	Northern Eurasia	51	-2	-78	0.00	-0.02	-0.13	0.21	-0.20	-0.16	-0.36	0.31
9	Arctic Eurasia	98	-6	-80	-0.02	-0.01	-0.12	0.26	-0.29	-0.12	-0.42	0.37
10	Central Africa	48	-3	-78	0.01	0.00	-0.17	0.19	-0.21	-0.18	-0.41	0.38
11	Southern Africa	79	-25	-48	-0.04	0.03	0.11	-0.22	-0.14	-0.13	-0.36	0.32
12	South America	32	-3	-43	-0.09	0.05	0.09	-0.05	-0.28	0.06	-0.39	0.29
13	Western US and Canada	53	-7	-82	-0.00	-0.02	-0.08	0.19	-0.20	-0.19	-0.41	0.30

Table 1: The lag time of the dynamical forcings [weeks] (in columns 3-5); and the best-fit coefficients of the constant term (in column 6), of the present-day Niño3.4, DMI and NAO (in columns 7-9), of the lagged Niño3.4, DMI and NAO (in columns 10-12), and the associated R squared (in column 13), of the multi-linear regression model. A positive lag means that the NO_2 lags behind the dynamical forcings, and vice versa a negative lag. Coefficients of the non-constant terms are marked in red when they contribute 10% or more to the total regression weighting.

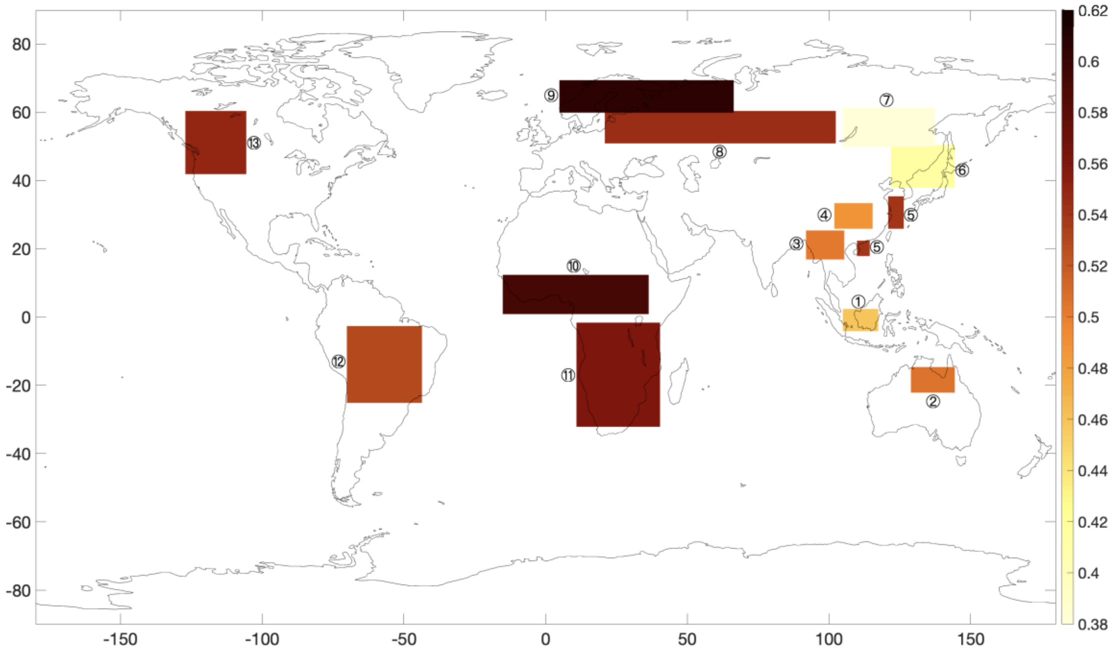

Figure 3: Map of reconstructed normalized variability using the respective best fit multi-linear regression model from each region. Note that this fraction represents the amount of the total variability of the NO_2 column measurements reproduced by the climate variables.

4. Discussion and Conclusions

The approach employed here successfully finds strong relationships between some extreme climate events and resulting chemical extreme events over the 14 years from 2004 to 2017. First, we determine that El Niño is the dominant term contributing to the variability of extremes in NO_2 over Siberia, which has not been previously reported in literature. On top of this, our multi-regression model demonstrates that the El Niño always impacts on future loadings of NO_2 in all studied regions, with its most significant impact (about 34 percent) occurring in both Northern Australia and Northern Southeast Asia when lags of 91 weeks and 7 weeks are applied respectively. Conversely, we find that the El Niño does not have a significant correlation on the extreme NO_2 columns measured over Indonesia, even though many previous works have stated that it is the major driving force between the fires observed in the Maritime Continent. This combination of findings is an important conclusion and warrants further study to understand more deeply the driving forces between these two highly variable and significant phenomena.

The IOD is found to dominate the NO_2 variability in many places in the world, including Indonesia, Northern Australia and South America. In our multi-regression model, the IOD lags behind the NO_2 columns in all regions except Northern Australia, where there is instead a possible proposed connection between the IOD and the emissions of NO_2 or other species co-emitted with NO_2 from biomass burning (i.e. heat or aerosols). The largest influence of the IOD is observed over Populated Northern China (also about 34 percent), when a lag of 7 weeks is applied.

The NAO influences the NO_2 columns across the globe in an overall wavelike manner, and plays a dominant role over most studied regions, including Northern Southeast Asia, Southern China Sea and Land, Populated Northern China, Northern and Arctic Eurasia, Central and Southern Africa and Western United States and Canada. Moreover, in the statistical multi-regression model, the NAO is found to lag behind almost all studied regions except Populated Northern China, which means that NO_2 along with other species co-emitted (including heat and aerosols) may also pose a significant feedback on the NAO. It is most significantly influenced over South America (found to contribute 42 percent), when a lag of 43 weeks is applied.

Over all of the non-heavily populated regions except for Siberia, we find that the climate variability is responsible for 50% to 60% of the total variability in measured NO_2 column loadings. Even in urban regions such as Indonesia and China the contribution is still more than 40%. Based on these results, it is suggested that the community look deeper into the roles of multiple dynamical forcings simultaneously acting on pollution extremes, as well as the possibility that extremes in pollution may have an impact on modulation of some of the largest global-scale dynamical systems.

Acknowledgments

We acknowledge the PIs of NASA OMI (https://disc.gsfc.nasa.gov/mirador-guide?tree=project&project=OMI) and NOAA (https://stateoftheocean.osmc.noaa.gov/sur/pac/

https://stateoftheocean.osmc.noaa.gov/sur/ind/ https://www.cpc.ncep.noaa.gov/products/precip/CWlink/pna/nao.shtml) for providing the remote sensing measurements and data. The work was supported by the Chinese National Young Thousand Talents Program (Project 41180002), the Chinese National Natural Science Foundation (Project 41030028), and the Guangdong Provincial Young Talent Support Fund (Project 42150003). All data currently in supplements, figures and tables is available at https://doi.org/10.6084/m9.figshare.c.4734440

References

Aragão, L. E. O. C., Anderson, L. O., Fonseca, M. G., Rosan, T. M., Vedovato, L. B., Wagner, F. H., . . . Saatchi, S. (2018). 21st Century drought-related fires counteract the decline of Amazon deforestation carbon emissions. *Nature Communications, 9*(1), 536. doi:10.1038/s41467-017-02771-y

Bollasina, M. A., Ming, Y., & Ramaswamy, V. (2011). Anthropogenic Aerosols and the Weakening of the South Asian Summer Monsoon. *Science, 334*(6055), 502-505. doi:10.1126/science.1204994

Bollasina, M. A., Ming, Y., & Ramaswamy, V. (2013). Earlier onset of the Indian monsoon in the late twentieth century: The role of anthropogenic aerosols. *Geophysical Research Letters, 40*(14), 3715-3720. doi:10.1002/grl.50719

Chen, S., Guo, J., Song, L., Cohen, J. B., & Wang, Y. (2019a). Temporal disparity of the atmospheric systems contributing to interannual variation of wintertime haze pollution in the North China Plain. *International Journal of Climatology, 0*(0). doi:10.1002/joc.6198

Chen, S., Guo, J., Song, L., Li, J., Liu, L., & Cohen, J. B. (2019b). Inter-annual variation of the spring haze pollution over the North China Plain: Roles of atmospheric circulation and sea surface temperature. *International Journal of Climatology, 39*(2), 783-798. doi:10.1002/joc.5842

Cohen, J. B. (2014). Quantifying the occurrence and magnitude of the Southeast Asian fire climatology. *Environmental Research Letters, 9*(11), 114018. doi:10.1088/1748-9326/9/11/114018

Cohen, J. B., Ng, D. H. L., Lim, A. W. L., & Chua, X. R. (2018). Vertical distribution of aerosols over the Maritime Continent during El Niño. *Atmos. Chem. Phys., 18*(10), 7095-7108. doi:10.5194/acp-18-7095-2018

Cohen, J. B., Prinn, R. G., & Wang, C. (2011). The impact of detailed urban-scale processing on the composition, distribution, and radiative forcing of anthropogenic aerosols. *Geophysical Research Letters, 38*(10). doi:10.1029/2011gl047417

Cohen, J. B., & Wang, C. (2014). Estimating global black carbon emissions using a top-down Kalman Filter approach. *Journal of Geophysical Research: Atmospheres, 119*(1), 307-323. doi:10.1002/2013jd019912

DeWitt, H. L., Gasore, J., Rupakheti, M., Potter, K. E., Prinn, R. G., Ndikubwimana, J. D. D., . . . Safari, B. (2019). Seasonal and diurnal variability in O3, black carbon, and CO measured at the Rwanda Climate Observatory. *Atmos. Chem. Phys., 19*(3), 2063-2078. doi:10.5194/acp-19-2063-2019

Diaz, H., & Markgraf, V. (Eds.). (2000). *El Niño and the Southern Oscillation: Multiscale Variability and Global and Regional Impacts*. Cambridge Univ. Press, Cambridge, U. K.

DiNezio, P. N., Deser, C., Karspeck, A., Yeager, S., Okumura, Y., Danabasoglu, G., . . . Meehl, G. A. (2017). A 2 Year Forecast for a 60–80% Chance of La Niña in 2017–2018. *Geophysical Research Letters, 44*(22), 11,624-611,635. doi:10.1002/2017GL074904

Field, R. D., van der Werf, G. R., Fanin, T., Fetzer, E. J., Fuller, R., Jethva, H., . . . Worden, H. M. (2016). Indonesian fire activity and smoke pollution in 2015 show persistent nonlinear sensitivity to El Niño-induced drought. *Proceedings of the National Academy of Sciences, 113*(33), 9204. doi:10.1073/pnas.1524888113

Grandey, B. S., Yeo, L. K., Lee, H.-H., & Wang, C. (2018). The Equilibrium Climate Response to Sulfur Dioxide and Carbonaceous Aerosol Emissions From East and Southeast Asia. *Geophysical Research Letters, 45*(20), 11,318-311,325. doi:10.1029/2018GL080127

Guo, J., Li, Y., Cohen, J. B., Li, J., Chen, D., Xu, H., . . . Zhai, P. (2019). Shift in the Temporal Trend of Boundary Layer Height in China Using Long-Term (1979–2016) Radiosonde Data. *Geophysical Research Letters, 46*(11), 6080-6089. doi:10.1029/2019GL082666

Hurrell, J. W. (1995). Decadal Trends in the North Atlantic Oscillation: Regional Temperatures and Precipitation. *Science, 269*(5224), 676. doi:10.1126/science.269.5224.676

Hurrell, J. W., Kushnir, Y., Ottersen, G., & Visbeck, M. (2003). *The North Atlantic Oscillation* (Vol. 134).

Ichoku, C., Giglio, L., Wooster, M. J., & Remer, L. A. (2008). Global characterization of biomass-burning patterns using satellite measurements of fire radiative energy. *Remote Sensing of Environment, 112*(6), 2950-2962. doi:10.1016/j.rse.2008.02.009

Jin, Q., & Wang, C. (2017). A revival of Indian summer monsoon rainfall since 2002. *Nature Climate Change, 7*, 587. doi:10.1038/nclimate3348

Kim, D., Chin, M., Remer, L. A., Diehl, T., Bian, H., Yu, H., . . . Stockwell, W. R. (2017). Role of surface wind and vegetation cover in multi-decadal variations of dust emission in the Sahara and Sahel. *Atmospheric Environment, 148*, 282-296. doi:10.1016/j.atmosenv.2016.10.051

Knippertz, P., Evans, M. J., Field, P. R., Fink, A. H., Liousse, C., & Marsham, J. H. (2015). The possible role of local air pollution in climate change in West Africa. *Nature Climate Change, 5*, 815. doi:10.1038/nclimate2727

Lan, R. Y., Cohen, J. B., Lin, C. Y., & Ng, D. H. L. (2019). Southeast Asian Biomass Burning Emissions in 2016 is More than Double Present Inventories, Largest in OMI Measurement History. SUBMITTED and UNDER REVIEW.

Leung, F.-Y. T., Logan, J. A., Park, R., Hyer, E., Kasischke, E., Streets, D., & Yurganov, L. (2007). Impacts of enhanced biomass burning in the boreal forests in 1998 on tropospheric chemistry and the sensitivity of model results to the injection height of emissions. *Journal of Geophysical Research: Atmospheres, 112*(D10). doi:10.1029/2006jd008132

Lin, C. Y., Cohen, J. B., Wang, S., Lan, R. Y., Deng, W. Z., Zhang, Y. L., & Liang, H. F. (2019). New Approach to Understanding the Vertical Distribution of Biomass Burning Carbon Monoxide Based on Climatological MOPITT Vertical Measurements. SUBMITTED and UNDER REVIEW.

Marlier, M. E., DeFries, R. S., Voulgarakis, A., Kinney, P. L., Randerson, J. T., Shindell, D. T., . . . Faluvegi, G. (2013). El Niño and health risks from landscape fire emissions in southeast Asia. *Nature Climate Change*, *3*(2), 131-136. doi:10.1038/nclimate1658

Martin, V. M., Kahn, R. A., Logan, J. A., Paugam, R., Wooster, M., & Ichoku, C. (2012). Space-based observational constraints for 1-D fire smoke plume-rise models. *Journal of Geophysical Research: Atmospheres, 117*(D22). doi:10.1029/2012jd018370

NOAA Climate Prediction Center Internet Team (2005). *North Atlantic Oscillation (NAO) Map (Positive Phase)*. NOAA Center for Weather and Climate Prediction Climate Prediction Center. 5830 University Research Court College Park, Maryland 20740, USA. Retrieved from https://www.cpc.ncep.noaa.gov/data/teledoc/nao_map.shtml.

Persad, G. G., Ming, Y., & Ramaswamy, V. (2014). The role of aerosol absorption in driving clear-sky solar dimming over East Asia. *Journal of Geophysical Research: Atmospheres, 119*(17), 10,410-410,424. doi:10.1002/2014jd021577

Reid, J. S., Xian, P., Hyer, E. J., Flatau, M. K., Ramirez, E. M., Turk, F. J., . . . Maloney, E. D. (2012). Multi-scale meteorological conceptual analysis of observed active fire hotspot activity and smoke optical depth in the Maritime Continent. *Atmos. Chem. Phys., 12*(4), 2117-2147. doi:10.5194/acp-12-2117-2012

Saji, N. H., Goswami, B. N., Vinayachandran, P. N., & Yamagata, T. (1999). A dipole mode in the tropical Indian Ocean. *Nature, 401*(6751), 360-363. doi:10.1038/43854

Shen, L., Mickley, L. J., Leibensperger, E. M., & Li, M. (2017). Strong Dependence of U.S. Summertime Air Quality on the Decadal Variability of Atlantic Sea Surface Temperatures. *Geophysical Research Letters, 44*(24), 12,527-512,535. doi:10.1002/2017GL075905

Siegert, F., Ruecker, G., Hinrichs, A., & Hoffmann, A. A. (2001). Increased damage from fires in logged forests during droughts caused by El Niño. *Nature, 414*(6862), 437-440. doi:10.1038/35106547

Sun, W.-Y., Yang, K. J.-S., & Lin, N.-H. (2013). Numerical Simulations of Asian Dust-Aerosols and Regional Impact on Weather and Climate- Part II: PRCM-Dust Model Simulation. *Aerosol and Air Quality Research, 13*(6), 1641-1654. doi:10.4209/aaqr.2013.06.0208

Tosca, M. G., Randerson, J. T., Zender, C. S., Nelson, D. L., Diner, D. J., & Logan, J. A. (2011). Dynamics of fire plumes and smoke clouds associated with peat and deforestation fires in Indonesia. *Journal of Geophysical Research: Atmospheres, 116*(D8). doi:10.1029/2010jd015148

Tsigaridis, K., Daskalakis, N., Kanakidou, M., Adams, P. J., Artaxo, P., Bahadur, R., . . . Zhang, X. (2014). The AeroCom evaluation and intercomparison of organic aerosol in global models. *Atmos. Chem. Phys., 14*(19), 10845-10895. doi:10.5194/acp-14-10845-2014

Velasco, E., & Rastan, S. (2015). Air quality in Singapore during the 2013 smoke-haze episode over the Strait of Malacca: Lessons learned. *Sustainable Cities and Society, 17*, 122-131. doi:10.1016/j.scs.2015.04.006

Wilkins, E. T. (1954). Air Pollution and the London Fog of December, 1952. *Journal of the Royal Sanitary Institute*, *74*(1), 1-21. doi:10.1177/146642405407400101